International Journal of Automotive Technology, Vol. 8, No. 4, pp. 483–491 (2007)

1229-9138/2007/035-11

INVESTIGATION OF A STRESS FIELD EVALUATED BY ELASTIC-PLASTIC ANALYSIS IN DISCONTINUOUS COMPOSITES

H. G. KIM*

Department of Mechanical and Automotive Engineering, Jeonju University, Cheonbuk 560-759, Korea

(Received 22 February 2007; Revised 6 July 2007)

ABSTRACT–A closed form solution of a composite mechanics system is performed for the investigation of elastic-plastic behavior in order to predict fiber stresses, fiber/matrix interfacial shear stresses, and matrix yielding behavior in short fiber reinforced metal matrix composites. The model is based on a theoretical development that considers the stress concentration between fiber ends and the propagation of matrix plasticity and is compared with the results of a conventional shear lag model as well as a modified shear lag model. For the region of matrix plasticity, slip mechanisms between the fiber and matrix which normally occur at the interface are taken into account for the derivation. Results of predicted stresses for the small-scale yielding as well as the large-scale yielding in the matrix are compared with other theories. The effects of fiber aspect ratio are also evaluated for the internal elastic-plastic stress field. It is found that the incorporation of strong fibers results in substantial improvements in composite strength relative to the fiber/matrix interfacial shear stresses, but can produce earlier matrix yielding because of intensified stress concentration effects. It is also found that the present model can be applied to investigate the stress transfer mechanism between the elastic fiber and the elastic-plastic matrix, such as in short fiber reinforced metal matrix composites.

KEY WORDS : Metal matrix composite, Slip, Elastic-plastic analysis, Fiber stress, Interfacial shear stress, Fiber aspect ratio

1. INTRODUCTION

Vehicle weight reduction has been of great interest to the automotive industry (Park *et al.*, 2005). Metal matrix composite are one of the most promising substitutes as a structural materials for many automotive and aerospace parts and for other applications (Agarwal *et al.*, 1980; Taya and Arsenault, 1989). Shear lag theory is one of the most popular models for these composites because of its simplicity (Agarwal *et al.*, 1974; Clyne, 1989; Cox, 1952). However, the major shortcoming of conventional shear lag (CSL) theory is that it is not able to provide sufficient accuracy in stress prediction when the fiber aspect ratio is small (Kim, 1998; Nardone and Prewo, 1986; Starink and Syngellakis, 1999). Accordingly, Nardone and Prewo (1986) attempted to modify the CSL by taking into account the tensile load transfer from the matrix to the discontinuous reinforcement. Their modified shear lag (MSL) model fits the experimental data well for prediction of yield strength of composites though it is limited by the assumption that the fiber stress has a constant value after matrix yielding, which shows the elastic-plastic composite behavior somewhat differently.

*Corresponding author. e-mail: hkim@jj.ac.kr

On the other hand, it has been proposed that the composite strengthening results from an increased dislocation density in the matrix due to a difference in the thermal expansion between the fiber and the matrix (Taya and Arsenault, 1987). However, the theory is unable to explain why the proportional limit of the composite remains similar to that of the matrix or why the strength of the composite is anisotropic. Obviously, the CSL model predicts composite yield strength values that are less than those observed, which indicates that the enhancement of increased dislocation density of the matrix is not the fundamental composite strengthening mechanism but that it can be one of the strengthening mechanisms.

Taya and Arsenault (1989) also proposed an elastic model that considers reinforced fiber end stress as the average matrix stress, but it is limited in the assumption that neglects the stress concentration effects between fiber ends; in addition, it does not have the capability to be applied to elastic-plastic behavior. There have been more attempts, such as those of Clyne (1989), Ji and Wang (2000), Jiang *et al.* (1998) Starink and Syngellakis (1999), though all of these models have shortcomings in complicated formulation or elastically limited derivation. Recently, Kim (2005) proposed the new shear lag (NSL) model which considers the stress concentration effects

between fiber ends for the behavior of the elastic fiber and elastic matrix in order to investigate fiber volume effects on the composite modulus.

In this paper, the CSL model is extended to the elastic-plastic behavior as a continuum approach in order to extend applications to metal matrix composite materials. The main effect of stress concentration is referred to the modulus ratio between the fiber and matrix as reported in the previous study (Kim *et al.*, 2005). The fiber stress, fiber/matrix interfacial shear stress and the onset of composite strain values are calculated by implementing not only the NSL model but also the CSL and MSL models. It is found that the NSL model is capable of correctly predicting the values of a local fiber stress variations as well as fiber/matrix interfacial shear stresses in the small fiber aspect ratio regime for the elastoplastic behavior.

2. FORMULATION OF CLOSED FORM SOLUTION FOR ELASTIC-PLASTIC STRESS ANALYSIS

In short fiber composites, loads are not directly applied to the fibers but are applied to the matrix and transferred to the fibers through the fiber ends as well as through the cylindrical surface of the fiber. A micromechanical model is described as follows. The representative volume element (RVE) is modeled under the assumption of perfect bonding between the fiber and the matrix. The RVE concept is described for an effective modeling in a previous engineering application (Kim, 2006). The short fibers are considered to be uniaxially aligned with the stress applied in the axial direction of the fibers. The axial direction is coordinated by z-axis and fiber diameter is defined by *d*. Figure 1, in general, describes the elastic-plastic model and associated stresses. The proposed composite unit cell showing the unstrained and strained RVE in a discontinuous composite is depicted in Figure 1(a) and (b). Hence, the fiber radius is fixed as unit length, i.e., $r_f = 1$, so that the aspect ratio, $s(=l/r_f)$, has the same length as the normalized fiber distance. Slip between the fiber and the matrix will normally take place by an interfacial shear stress which varies along the fiber length. The diameters of the fiber and RVE are r_f and R, and σ_f is fiber axial stress, respectively. Likewise, the shear stresses of the fiber surface and arbitrary surrounding matrix are τ_i and τ, respectively. The CSL model is based on the following two equations (Cox, 1952).

$$2\pi r\tau dz = 2\pi r_f \tau_i dz \quad (\text{or } \tau = r_f\tau_i/r) \tag{1}$$

$$2\pi r_f \tau_i dz = \pi r^2 d\sigma_f \tag{2}$$

Hence, Equation (2) shows that the shear forces acting on the fibers are equivalent to the tensile force within the fiber. The above relationship can result in the governing differential equation in association with the combination

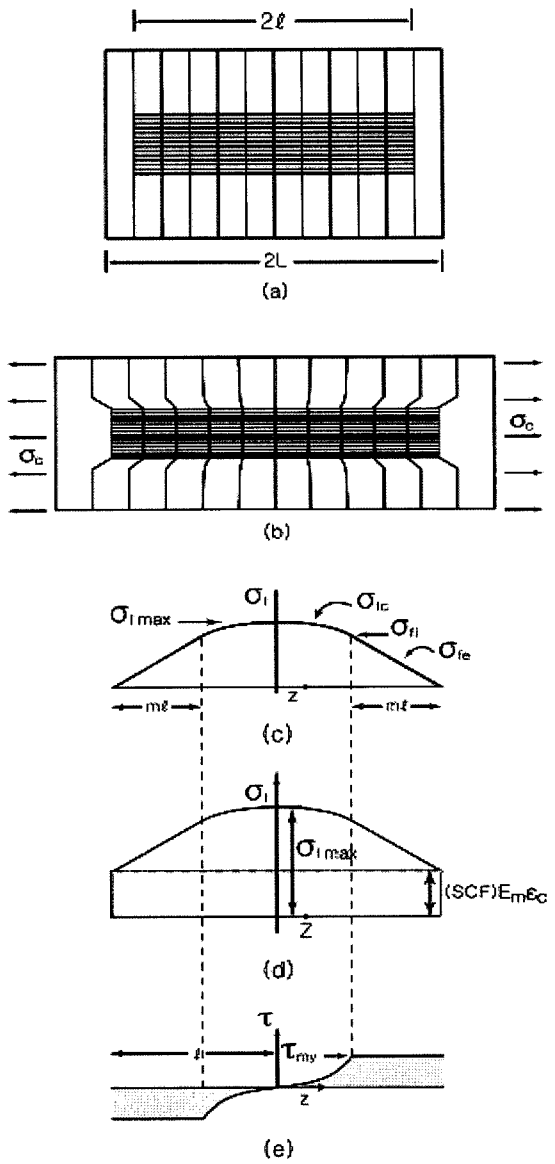

Figure 1. Schematic diagram of a single fiber composite model: (a) RVE with fiber length of $2l$ and RVE cell length of $2L$; (b) shapes of strained RVE which shows slip mechanism at the fiber/matrix interface; (c) fiber stress of the CSL model in elastic-plastic regime; (d) fiber stress of the NSL model in elastic-plastic regime; (e) fiber/matrix interfacial shear stress in elastic-plastic regime.

of equilibrium conditions and Hooke's law (Cox, 1952; Kim, 1998). Based on the CSL model, the governing differential equation of the composite is given by

$$\frac{d^2\sigma_f}{dz^2} = \frac{n^2}{r^2}(\sigma_f - E_f\varepsilon_c) \tag{3}$$

where E is the elastic modulus, ε is the strain, and n is the

dimensionless parameter as can be seen in Equation (4). The subscripts f, m, and c indicate fiber, matrix and composite respectively. The parameter n is dimensionless and is as below.

$$n^2=\frac{2E_m}{E_f(1+\nu_m)\ln\left(\frac{P_f}{V_f}\right)} \tag{4}$$

where ν_m is the Poisson's ratio of the matrix, P_f is the packing factor, and V_f is the fiber volume fraction. This has the solution of Equation (5) and (6) for the fiber axial stress and the fiber/matrix interfacial shear stress in the elastic fiber/matrix behavior.

$$\sigma_f^{CSL}=E_f\varepsilon_c\left\{1-\frac{\cosh(nz/r_f)}{2\cosh(ns)}\right\} \tag{5}$$

$$\tau_i^{CSL}=\frac{nE_f\varepsilon_c\sinh(nz/r_f)}{2\cosh(ns)} \tag{6}$$

However, it is observed that the prediction is underestimated because of the neglected stress intensification at the fiber ends, as shown in Figure 1 (Clyne, 1989; Jiang *et al.*, 1998; Starink and Syngellakis, 1999). Hence, fiber end stress, including stress concentration effects should be implemented as a boundary condition. Thus, Equation (7) has been derived for the more accurate fiber/matrix axial interfacial condition (Kim, 2005).

$$\sigma_i=\alpha_k E_m\varepsilon_c \quad \text{for } z=\pm l \tag{7}$$

where α_k is a stress concentration factor (SCF) between the fiber end and the matrix, which can be evaluated as a square root function of the modulus ratio (Kim, 2005). Thus, α_k can be expressed in Equation (8) as depicted in Figure 1(d).

$$\alpha_k=\sqrt{E_f/E_m} \tag{8}$$

By this formulation, the fiber axial stress and the fiber/matrix interfacial shear stress in the elastic regime are derived as follows.

$$\sigma_f^{NSL}=E_f\left\{1+\left(\sqrt{\frac{E_m}{E_f}}-1\right)\frac{\cosh(nz/r_f)}{\cosh(ns)}\right\}\varepsilon_c \tag{9}$$

$$\tau_i^{NSL}=\frac{nE_f(1-\sqrt{E_m/E_f})\sinh(nz/r_f)}{2\cosh(ns)}\varepsilon_c \tag{10}$$

For the extension to the elastic-plastic regime, on the other hand, Nardone and Prewo (1986) presented the MSL (Modified Shear Lag) model, which aims mainly to predict composite yield strength. However, their model is indeed a limiting case which occurs when the plastic front approaches the end of the fiber, so that the whole cylindrical interface is plastic and the interface adds a matrix yield stress contributing to the axial load transfer. Thus, their model includes the intrinsic limitation associated with large plastic strains. Their formulation for the fiber axial stress is as below.

$$\sigma_f^{MSL}=\sigma_i+2\tau_i\frac{(l-z)}{r_f} \tag{11}$$

where σ_i is the interfacial normal stress between fiber ends and τ_i is the interfacial shear stress between fiber and matrix. In their study, the prediction of the fiber/matrix interfacial shear stress is assumed to be half of the matrix yield stress. An effort has been made to overcome the limitation of being unable to express the elastic-plastic behavior.

In the case of matrices, in the above, if work hardening is neglected and if the fiber/matrix adhesion is perfect, the shear stress will be constant in the slip regions as shown in Figure 1(e), and equal to the shear yield stress of the matrix τ_{my}. The slip occurs over a length ml at both ends of the fiber, where m is a dimensionless parameter that depends on the applied stress, although Nardone and Prewo (1986) assumed that the slip occurs over a length l. Using the boundary conditions $\sigma_f=\sigma_{fi}$ at $z=l(1-m)$, σ_{fc} can be written as Equation (12). Hence, σ_{fi} is an interfacial fiber stress at the boundary between the elastic and plastic matrix region.

$$\sigma_{fc}=E_f\varepsilon_c+(\sigma_{fi}+E_f\varepsilon_c)\frac{\cosh(nz/r)}{\cosh(n\bar{s})} \tag{12}$$

where σ_{fc} is the fiber stress in the center region and $\bar{s}$ is the reduced aspect ratio. Hence, the relationship between $\bar{s}$ and s is expressed as below.

$$\bar{s}=s(1-m) \tag{13}$$

Rearranging and simplifying for the surface shear forces to be in equilibrium with the tensile forces in the fiber yields

$$\frac{d\sigma_{fe}}{dz}=-\frac{2\tau_{my}}{r_f} \tag{14}$$

where σ_{fe} is the fiber stress in the slip region and τ_{my} represents the matrix shear yield stress. The interfacial shear stress, τ_i, is constant at $\tau_i=\tau_{my}$. Assuming that, by the CSL model, normal stress does not transfer across the fiber ends, it can be set by $\sigma_f=0$ for $z=l$ resulting in Equation (15).

$$\sigma_{fd}^{CSL}=\frac{2\tau_{my}}{r_f}(l-z) \tag{15}$$

But this result is impractical for the short fiber case. Therefore, the boundary condition is redefined as $\sigma_{fe}=2\tau_{my}$ for $z=l$. Fiber stress in the slip region can be derived as Equation (16) by integrating Equation (14).

$$\sigma_{fe}^{NSL}=\frac{2\tau_{my}}{r_f}(l-z)+2\tau_{my} \tag{16}$$

and the value of σ_{fe}^{CSL} and σ_{fe}^{NSL} gives the following since

$\sigma_{fe}=\sigma_{fi}$ at $z=l(1-m)$.

$$\sigma_{fi}^{CSL}=2ms\tau_{my} \tag{17}$$

$$\sigma_{fi}^{NSL}=2(ms+1)\tau_{my} \tag{18}$$

where σ_{fi} is the fiber interfacial normal stress between the center and the end region. Hence, the fiber stress in the center region can be rearranged by Equations (19) and (20) for the CSL and NSL model respectively.

$$\sigma_{fc}^{CLS}=E_f\varepsilon_c+(2ms\tau_{my}-E_f\varepsilon_c)\frac{\cosh(nz/r)}{\cosh(n\bar{s})} \tag{19}$$

$$\sigma_{fc}^{NSL}=E_f\varepsilon_c+[2(ms+1)\tau_{my}-E_f\varepsilon_c]\frac{\cosh(nz/r)}{\cosh(n\bar{s})} \tag{20}$$

In the meantime, the MSL model is simplified without the above process so that the matrix yield stress may transfer to the fiber surface. This means that surrounding matrix must be in the region of plasticity and it results in Equation (11). The fiber stress calculated by the MSL model is linear, as can be found in Equation (11), and is independent of far field loading, and additionally presumes that fracture may occur at the fiber center with very large stress value as soon as matrix yielding occurs. On the other hand, the fiber/matrix interfacial shear stresses in the center region, τ_{ic}^{CLS}, τ_{ic}^{MSL}, and τ_{ic}^{NSL}, can be obtained by differentiating and substituting each fiber stress in the equilibrium condition, whereas those in the fiber end region, τ_{ic}^{CLS}, τ_{ic}^{MSL}, and τ_{ic}^{NSL} are merged to the same value of τ_{my} as follows.

$$\tau_{ic}^{CLS}=\frac{nE_f\varepsilon_f\sinh(nz/r_f)}{2\cosh(n\bar{s})} \tag{21}$$

$$\tau_{ic}^{MSL}=\tau_{my} \tag{22}$$

$$\tau_{ic}^{NSL}=\frac{nE_f(1-\sqrt{E_m/E_f})\varepsilon_c\sinh(nz/r_f)}{2\cosh(n\bar{s})} \tag{23}$$

$$\tau_{ic}^{CSL}=\tau_{ic}^{MSL}=\tau_{ic}^{NSL}=\tau_{my} \tag{24}$$

3. RESULTS AND DISCUSSION

The numerical results calculated by the above formula are concurrently compared to those of the CSL, MSL, and NSL models to investigate the stress distribution in the fiber and fiber/matrix interface. Material properties applied are E_m=70 GPa (matrix), E_f=480 GPa (fiber), ν_m=0.33, r_f=1 (unit length), and $P_f=2/\sqrt{3}$ (packing factor). Under this condition, the fiber stresses and fiber/matrix interfacial shear stresses are investigated by varying the fiber aspect ratio and composite strain. The far field composite strains are applied by ε_c=0.0040, ε_c=0.0044, ε_c=0.0048, ε_c=0.0052 and ε_c=0.0056 to examine the evolution of matrix plasticity in the case of V_f=20%. Fiber aspect ratios are varied from 4 to 10 to investigate the sensitivity of the stress values. In the end, the composite proportional limit is also investigated in association with the change of fiber volume fractions.

3.1. Fiber Axial Stresses

Figure 2 shows the internal fiber axial stresses while the

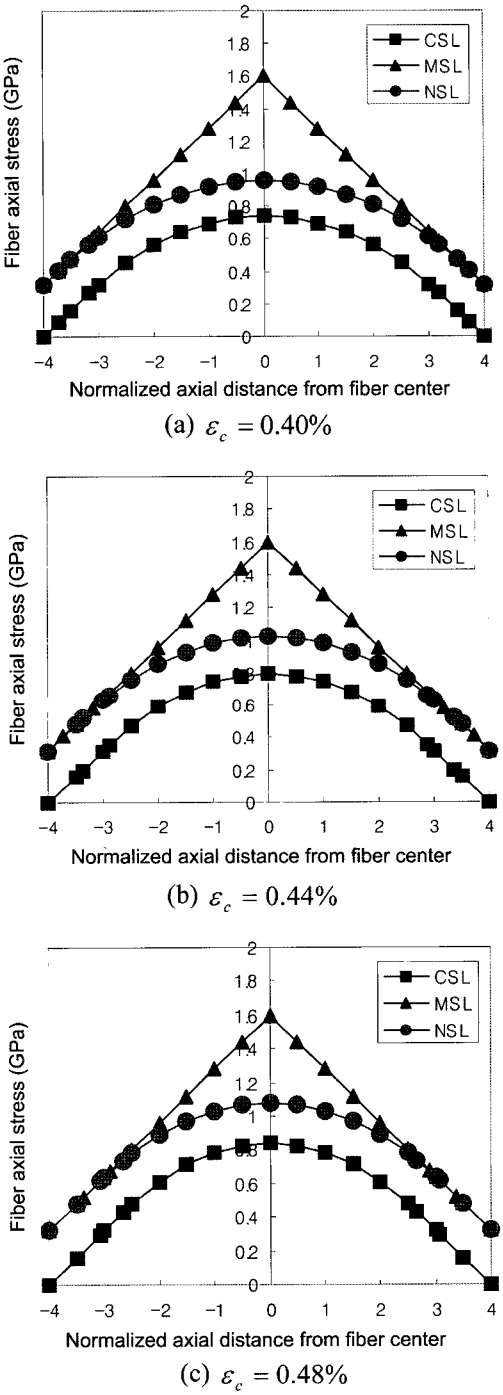

Figure 2. Prediction of fiber stresses and movement of slip points according to the increment of far field composite strain in the case of s=4 and V_f=20%.

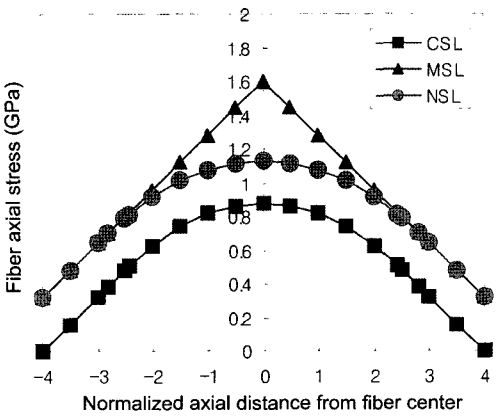

(d) $\varepsilon_c = 0.52\%$

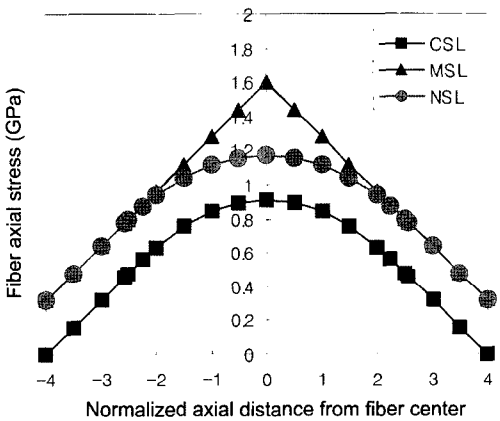

(e) $\varepsilon_c = 0.56\%$

Figure 2. Continued.

matrix evolves with elastic-plastic behavior, before matrix general yielding in the case of s=4 and V_f=20%. In all figures, the results of the NSL model fall between those of CSL and MSL models, whereas those of MSL model show an independent value of applied strain presenting an upper bound of fiber axial stresses. As described in Figure 2, the results of the CSL model obviously underestimate on account of neglecting fiber end stress or discontinuity. However, those of MSL overestimate due to the assumption that the whole cylindrical fiber/matrix interface is plastic and fiber ends also add to the axial load transfer when the plastic front approaches the end of the fiber. Figure 2 depicts that the MSL and NSL models show a great discrepancy, especially in the fiber center region, whereas that discrepancy becomes smaller as composite strain increases. The figures also show the predictions for movement of slip points, according to the increment of the far field composite strain, which indicate that slip points forward to the fiber center.

3.2. Fiber/Matrix Interfacial Shear Stresses

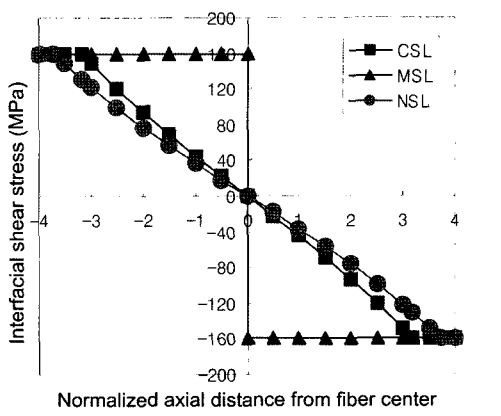

(a) $\varepsilon_c = 0.40\%$

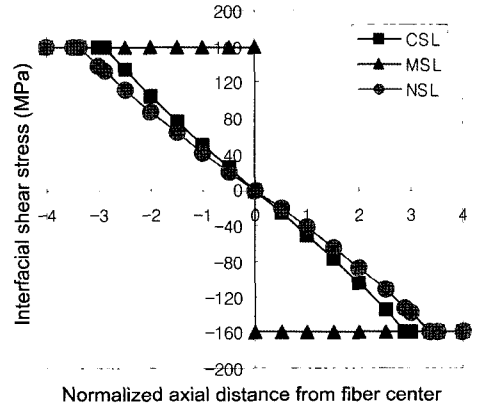

(b) $\varepsilon_c = 0.44\%$

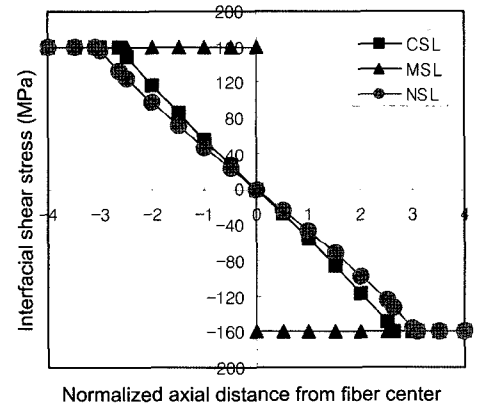

(c) $\varepsilon_c = 0.48\%$

Figure 3. Prediction of fiber/matrix interfacial shear stresses and movement of slip points according to the increment of far field composite strain in the case of s=4 and V_f=20%.

Figures 3(a) through (e) show the predictions for fiber/matrix interfacial shear stresses while the matrix evolves with elastic-plastic behavior, before matrix general yielding in the case of s=4 and V_f=20%. As is in the fiber

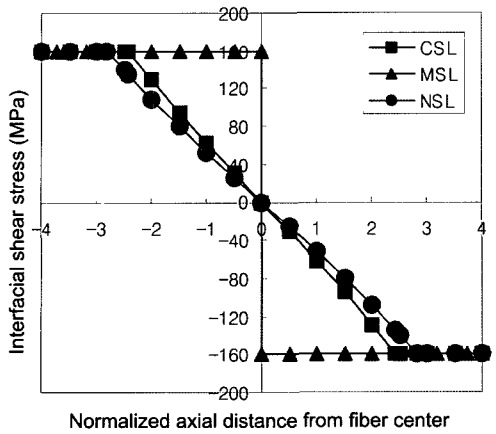

(d) $\varepsilon_c = 0.52\%$

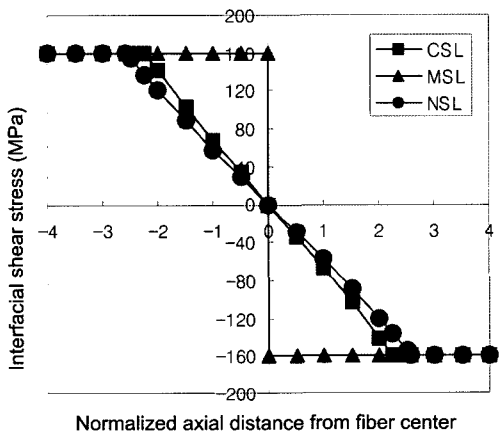

(e) $\varepsilon_c = 0.56\%$

Figure 3. Continued

stresses, the shear stress results of the NSL model also fall between those of CSL and MSL models, whereas the MSL model shows an independent value of applied strain which also gives an upper bound for fiber/matrix interfacial shear stresses. The results of CSL and NSL models show relatively little difference compared to the fiber axial stresses. Figure 3 also shows prediction of movement of slip points according to the increment of far field composite strain, which indicates that slip points forward to the fiber center.

3.3. Effects of Fiber Aspect Ratio

Figure 4, along with Figure 2(a), shows predictions for fiber axial stresses according to the fiber aspect ratio in the case of far field composite strain of ε_c=0.00040 and fiber volume fraction of 20%. Predicted values from the CSL and NSL models show that the fiber axial stress displays larger discrepancies as the fiber aspect ratio becomes smaller while those of the MSL model depict a steady value. Obviously, the fiber aspect ratio plays an important role in the fiber axial stresses as seen in the comparison of Figure 2(a) with Figure 4(c).

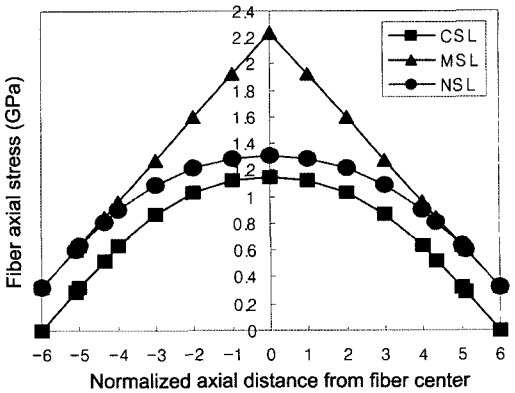

(a) s = 6

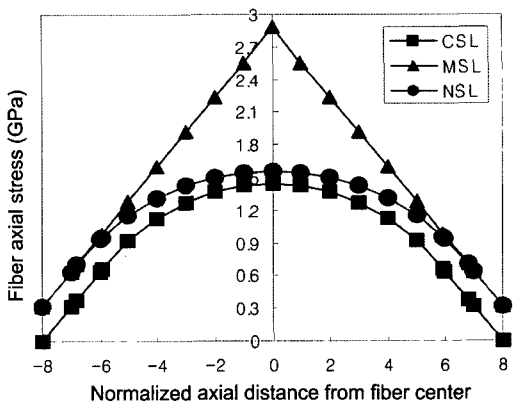

(b) s = 8

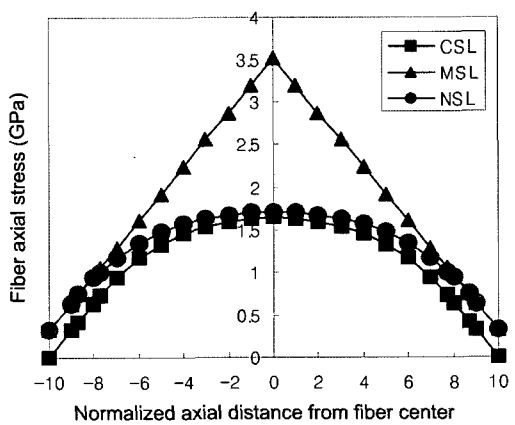

(c) s = 10

Figure 4. Prediction of fiber stresses according to the fiber aspect ratio in the case of far field composite strain of ε_c=0.40% and fiber volume fraction of 20%.

Figure 5, along with Figure 3(a), shows predictions for fiber/matrix interfacial shear stresses according to fiber aspect ratio in the case of far field composite strain of ε_c=0.0040 and fiber volume fraction of 20%. The results

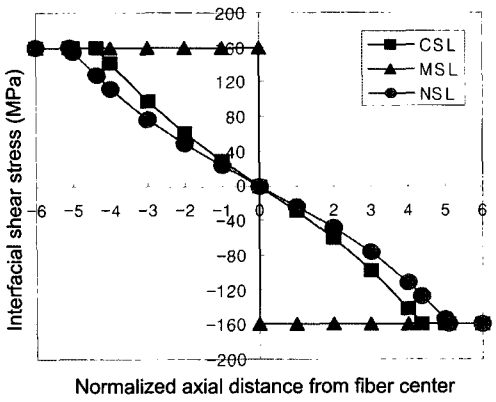

(a) s=6

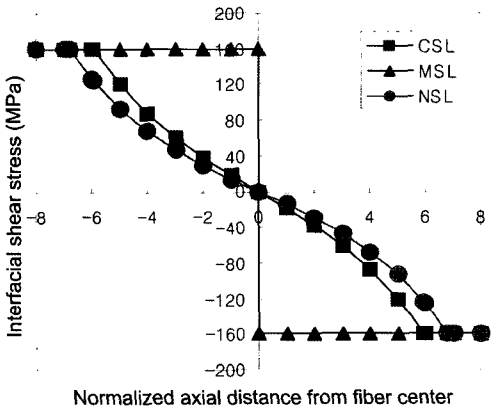

(b) s=8

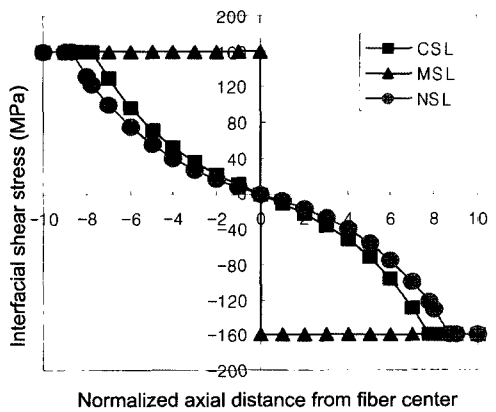

(c) s=10

Figure 5. Prediction of fiber/matrix interfacial shear stresses according to the fiber aspect ratio in the case of far field composite strain of ε_c=0.40% and fiber volume fraction of 20%.

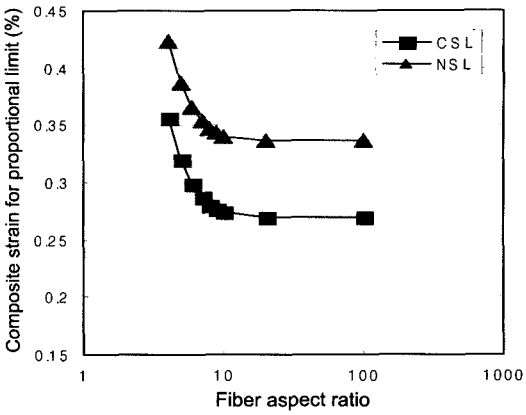

(a) $V_f = 10\%$

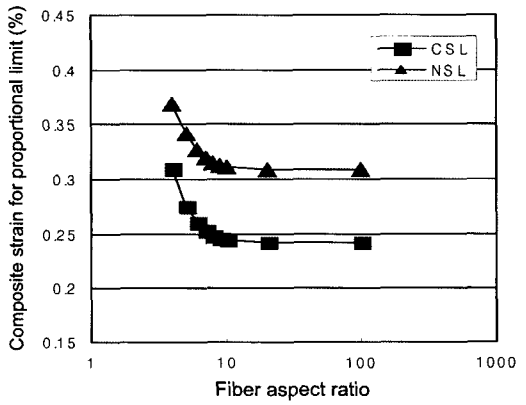

(b) $V_f = 20\%$

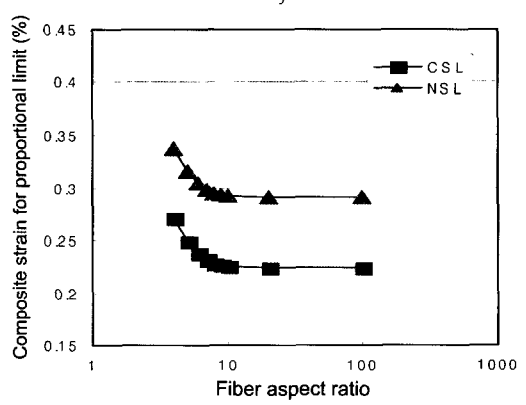

(c) $V_f = 30\%$

Figure 6. Prediction of composite strain for proportional limit according to the fiber aspect ratio in the case of fiber volume fraction of 10%, 20%, 30%, 40%, and 50%.

of the CSL and NSL models show relatively little difference compared to the fiber axial stresses while those of the MSL model depict a steady value. The fiber aspect ratio plays a relatively less important role in the increment of fiber/matrix interfacial shear stresses, as seen in the comparison of Figure 3(a) with Figure 5(c).

3.4. Composite Strain for Proportional Limit

The onset of slip in the matrix is determined analytically using the present model and is also compared with the conventional model. Figure 6 shows predictions of com-

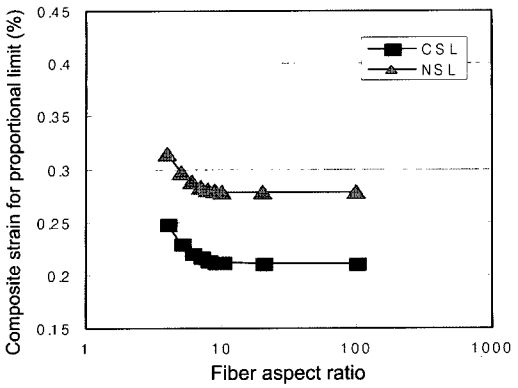

(d) $V_f = 40\%$

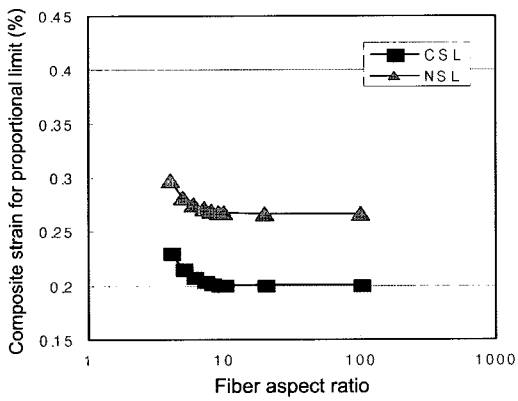

(e) $V_f = 50\%$

Figure 6. Continued

posite strain for the proportional limit according to the fiber aspect ratio in the case of fiber volume fraction of 10%, 20%, 30%, 40% and 50% respectively. Composite strains for the proportional limit of the CSL model is far lower than those of the NSL model in all cases. The rationale is that the NSL model takes into account the stress concentration effect at the fiber ends while the CSL model relies on shear stress in the whole, so that the CSL model triggers local yielding at an earlier stage than the NSL model. Composite strains for the proportional limit are also a strong function of fiber aspect ratio though saturation occurs at a fiber aspect ratio of 10. On the other hand, the fiber volume fraction plays an important role in plasticity evolution. In Figure 6, the range of composite strains for the proportional limit of fiber volume fraction 10% is shown as NSL model (0.42%~0.34%) and CSL model (0.36%~0.27%) while those of fiber volume fraction 10% are shown as NSL model (0.29%~0.26%) and CSL model (0.23%~0.20%) in the case of a short fiber like s=4. Accordingly, the decrease in the NSL model is nearly 30% (from 0.42% to 0.34%) and that of the CSL model is nearly 35% (from 0.36% to 0.23%) respectively. This phenomenon indicates that the localized matrix yielding is affected significantly by the fiber volume fraction as well as the fiber aspect ratio.

4. CONCLUSIONS

The shear lag model is extended to the elastic-plastic behavior as a continuum approach in order to apply it to metal matrix composite materials. Stress concentration effects are taken into account in order to derive a closed form solution. The present model (NSL) is compared to the conventional shear lag model (CSL) as well as the modified shear lag model (MSL). The results of the NSL model always fall between that of the CSL and MSL models. Some important conclusions investigated by the three models are as follows.

(1) The results of the NSL model fall between those of the CSL and MSL model, whereas those of the MSL model show an independent value for applied strain presenting an upper bound of fiber axial stresses.
(2) The fiber axial stress of the NSL model shows a great difference from that of the CSL and MSL models and is a strong function of the fiber aspect ratio.
(3) The fiber/matrix interfacial shear stresses of CSL and NSL show relatively little difference compared to the fiber axial stresses.
(4) Localized matrix yielding is affected significantly by the fiber volume fraction as well as the fiber aspect ratio.
(5) The slip points move forward to the fiber center region as the far field strain increases.

REFERENCES

Agarwal, B. D. and Broutman, L. J. (1980). *Analysis and Performance of Fiber Composites*. Johns Wiley and Sons. New York. 71–104.

Agarwal, B. D., Broutman, L. J. and Lifshitz, J. M. (1974). Elastic-plastic finite element analysis of short fiber composites. *Fib. Sci. Tech.*, **7**, 45–62.

Clyne, T. W. (1989). A simple development of the shear lag theory appropriate for composites with a relatively small modulus mismatch. *Mat. Sci. Eng. A*, **122**, 183–190.

Cox, H. L. (1952). The elasticity and strength of paper and other fibrous materials. *Brit. J. Appl. Phys.*, **3**, 72–79.

Ji, B. and Wang, T. (2000). Constitutive behaviors of discontinuous reinforced composites. *Key Eng. Mat.*, 177–180, 297–302.

Jiang, Z., Lian, J., Yang, D. and Dong, S. (1998). An analytical study of the influence of thermal residual stresses on the elastic and yield behaviors of short fiber-reinforced metal matrix composites. *Mat. Sci. Eng. A*, **248**, 256–275.

Kim, H. G. (1998). Analytical study on the elastic-plastic transition in short fiber reinforced composites. *J. Mechanical Science and Technology* **12**, **2**, 257–266.

Kim, H. G. (2005). Predictions of elastic properties in discontinuous composite materials. *Key Eng. Mat.*, 297–300, 1265–1269.

Kim, H. G., Kim, Y. S. and Shu, Z. (2006). Simulation of unit cell performance in the polymer electrolyte membrane fuel cell. *Int. J. Automotive Technology* **7**, **7**, 867–872.

Nardone, V. C. and Prewo, K. M. (1986). On the strength of discontinuous silicon carbide reinforced aluminum composites. *Scr. Metal.*, **20**, 43–48.

Park, Y. B., Lee, M. H. and Kim, H. Y. (2005). Design of adhesive bonded joint using aluminum sandwich sheet. *Int. J. Automotive Technology* **6**, **6**, 657–663.

Starink, M. J. and Syngellakis, S. (1999). Shear lag models for discontinuous composites: Fibre end stresses and weak interface layers. *Mat. Sci. Eng.* A, **270**, 270–277.

Taya, M. and Arsenault, R. J. (1987). A comparison between a shear lag type model and an Eshelby type model in predicting the mechanical properties of short fiber composite. *Scr. Metal.*, **21**, 349–354.

Taya, M. and Arsenault, R. J. (1989). *Metal Matrix Composites: Thermo-mechanical Behavior.* Pergamon Press. New York. 101–149.